JCTC Journal of Chemical Theory and Computation

Article

pubs.acs.org/JCTC

Singlet Exciton Diffusion in Organic Crystals Based on Marcus Transfer Rates

Vera Stehr,*[,†] Reinhold F. Fink,[‡] Bernd Engels,[¶] Jens Pflaum,[†] and Carsten Deibel[†]

[†]Physikalisches Institut, Universität Würzburg, 97074 Würzburg, Germany

[‡]Institut für Physikalische und Theoretische Chemie, Universität Tübingen, 72076 Tübingen, Germany

[¶]Institut für Physikalische und Theoretische Chemie, Universität Würzburg, 97074 Würzburg, Germany

ABSTRACT: Exciton diffusion is a critical step for energy conversion in optoelectronic devices. This spawns the desire for theoretical approaches that allow for fast but reliable determinations of the material-dependent exciton transport parameters. For this purpose, the Marcus theory, which is widely used in the context of charge transport, is adapted to exciton diffusion. In contrast to the common approach of calculating the exciton hopping rate via the coupling and the spectral overlap, this alternative approach is less costly, because, instead of the spectral overlap, only the reorganization energy is needed. To demonstrate the capability of the approach, the diffusion constants for naphthalene, anthracene, and diindenoperylene crystals are calculated and compared with both calculations conducted with the well-established exciton hopping rate, including coupling and spectral overlap, and with experimental data. These test calculations show that Marcus-based exciton diffusion properties tend to be too small but are qualitatively correct (i.e., they seem to be useful to predict trends). Nevertheless, for reliable results, high-level quantum chemical approaches are necessary for the computation of the reorganization energies. However, they have to be calculated only once. Coupling constants, which are needed for all pairs of monomers, have a considerably smaller influence, i.e., they can be computed by a lower level approach, which makes the method even less costly.

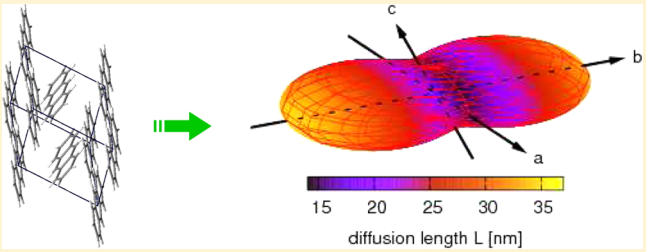

1. INTRODUCTION

Organic semiconductor devices are becoming more and more attractive, because of their low production costs, easy processability, and the advancing technological progress, especially in the field of light-emitting diodes (OLEDs),[1−3] organic field effect transistors (OFETs),[4−6] radio-frequency identification tags (RFIDs),[7,8] and solar cells,[9−13] to mention just a few. Because of the large exciton binding energy in organic materials (100−400 meV),[13−17] exciton diffusion is an important step for the energy conversion in organic solar cells. Dissociation into free charge carriers is only possible if the exciton reaches the donor/acceptor interface within its lifetime. Typical diffusion lengths are some tens of nanometers, while the absorption lengths of organic semiconductors are ∼80−200 nm,[18] which necessarily results in a compromise for the layer thickness. To facilitate the search for materials with larger diffusion lengths, theoretical approaches are needed which allow an easy and fast yet thorough estimation of diffusion lengths in promising materials.

Exciton transport in covalently bonded inorganic crystals is mainly described by band transport, which basically also holds for organic crystals.[15,19−22] However, the only weak van der Waals interactions lead to less rigidity of these molecular crystals, lattice vibrations are more pronounced in organic than in inorganic crystals. This strongly affects the long-range order on the relevant time scale for exciton motion and, therefore, can lead to a localization of charge carriers and excitons. At room temperature, it should be justifiable to assume that incoherent exciton transport takes place.[23,24] This was also shown in a previous work, which for naphthalene and anthracene showed an excellent agreement between the hopping model and experimental results.[25] In this work, we presented a protocol for a rate equation approach based on a Förster-like hopping equation to calculate exciton diffusion lengths.

Incoherent exciton transport is customarily described by thermally activated hopping models based on time-dependent perturbation theory.[25−30] A derivation of this is the Marcus theory,[31,32] which is normally applied in the context of charge transport.[27,33−35] Here, we adapt this approach to exciton transport.

The paper is organized as follows: Section 2.1 describes the hopping approach and the adaption of the Marcus theory to exciton transport. Section 2.2 explains the approach used for the transport calculations. In section 2.3, the equations and the quantum chemical methods used to calculate the parameters needed for the hopping rate are explained. Section 3 presents the results and discusses the influence of different quantum chemical approaches on the accuracy of the computed exciton

Received: October 25, 2013
Published: January 30, 2014

   dx.doi.org/10.1021/ct500014h | J. Chem. Theory Comput. 2014, 10, 1242−1255

diffusion parameters. Calculations on naphthalene and anthracene are taken as example, because the medium size of these molecules makes it possible to use numerically expensive methods. Furthermore, results for diindenoperylene[36] are shown, which is a highly promising candidate for application in organic electronics, because of its ambipolar charge transport characteristics,[23] its long-range ordered structure in thin films,[37] and the relatively high charge carrier mobilities,[38] as well as exciton diffusion length.[24,39]

2. THEORY AND MODELING

2.1. The Marcus Hopping Model. In this work, a hopping mechanism is assumed for the motion of the excitons. Based on Fermi's Golden rule, the jump rate from site i to j can be expressed as[25,26,29,40,41]

$$\nu_{ji} = \frac{2\pi}{\hbar} V_{ji}^2 J \tag{1}$$

where V_{ji} is the electronic coupling parameter, $\hbar$ is the reduced Planck constant, and J is the Franck−Condon weighted density of states (FCWD),[25]

$$J = \int D^{\mathrm{abs}}(E) D^{\mathrm{em}}(E)\, \mathrm{d}E \tag{2}$$

which accounts for the vibrations of the molecules and is approximated by the spectral overlap of the densities of states $D^{\mathrm{em}}(E)$ of the donor emission and $D^{\mathrm{abs}}(E)$ of the acceptor absorption.

In order to calculate J, the vibrational wave functions of both the ground and the excited state of the molecule must be evaluated. Commonly, the harmonic approximation is used,[42,43] which is, however, doubtful for low-frequency vibrations. For that reason, the low-frequency modes are usually fitted to measured spectra.[28,29] In the general case, the normal modes of the ground state and excited state mix, which must be taken into account by a Duschinsky rotation,[43,44] which complicates the calculations significantly. Because of these difficulties, sometimes experimental values for J are used instead.[30]

As an alternative approach, we have adapted the Marcus theory,[31,32] which is already widely and successfully used for charge transport,[35,45−51] to exciton transport. The Marcus hopping rate reads as follows:[31−33,40]

$$\nu_{ji} = \frac{V_{ji}^2}{\hbar} \sqrt{\frac{\pi}{\lambda k_{\mathrm{B}} T}} \exp\left(-\frac{\lambda}{4 k_{\mathrm{B}} T}\right) \tag{3}$$

where λ is the reorganization energy of the neutral donor−acceptor complex due to the exciton transfer, T the temperature, and k_{B} the Boltzmann constant. Similarities between eqs 1 and 3 were already denoted in refs 52 and 53.

The Marcus theory was originally derived for outer sphere electron transfer in solvents,[31] and it describes a nonadiabatic transfer where the charge carrier is localized at the donor or acceptor molecule, respectively. As observed in eq 1, which is frequently used for exciton motion,[25,28−30,54] this theory stems from time-dependent perturbation theory, suggesting a straightforward transfer to exciton transport.

From the viewpoint of quantum chemical calculations, the Marcus theory is much easier, since, instead of explicitly calculating the spectral overlap for the Franck−Condon factors, it is sufficient to calculate the reorganization energy (λ), which can be done with much less effort, since no frequency calculations but only geometry optimizations of the ground state and the excited state are necessary. (The calculation of λ is explained in detail in section 2.3.)

Treating the coupling as a perturbation requires V_{ji} to be small, compared to $\lambda/4$, which corresponds to the activation energy for the charge or the exciton to change place (weak coupling regime[53]). Because of the smaller couplings and the larger reorganization energies, this condition is satisfied even better for excitons than for charges. Furthermore, the relaxation (the geometric reorganization) has to be fast, in comparison with the transfer, so that the system can be assumed in its thermal equilibrium during the transfer. In addition, the theory is restricted to the high-temperature case since tunneling is neglected completely and the molecular vibrations are treated classically, thus requiring $k_{\mathrm{B}}T \gg \hbar\omega$. This condition is often not met for the high-frequency intramolecular vibrational modes. However, despite all imperfections, the Marcus theory has been proven to yield good results for charge transfer in organic crystals[35,45−51] and one can certainly assume that this theory is suitable for the purpose of a qualitative exciton transport analysis as well.

The interaction between excitons and phonons is partially considered by the reorganization energy. Because of the weak van der Waals interactions between organic molecules, it can be divided into an internal (intramolecular) and an external (intermolecular) part, i.e., $\lambda = \lambda_{\mathrm{int}} + \lambda_{\mathrm{ext}}$. The intramolecular reorganization energy λ_{int} is due to the geometry changes of the donor and the acceptor monomer upon exciton transfer. The external reorganization energy λ_{ext} covers the energetic changes concerning the surrounding, caused by the lattice distortion.

For charge transport in oligoacenes, λ_{ext} was shown to be ∼1 order of magnitude smaller than λ_{int}.[55,56] For exciton transport, the internal reorganization energies are typically larger than those for charge transport, because an electron from a bonding orbital is lifted into an antibonding orbital, leading to a stronger change of the molecular geometry. In contrast, the external reorganization energy is expected to be smaller in the case of excitons since they are neutral and do not lead to a strong polarization of their surroundings as in the case of charge carriers. That is why the external reorganization energy is neglected in this paper and only the internal reorganization energy of the monomer under vacuum is used for λ.

2.2. Transport Calculations. It has been shown that averaging by means of a simple diffusion rate equation based on the jump rates and the squared jump distance possibly leads to an overestimation of the diffusion constant.[25,35] This can be circumvented by determining the diffusion coefficient via the Einstein relation from the mobility. The latter can be calculated efficiently by introducing a drift term[25] into the Marcus rate equation (eq 3), resulting in

$$\begin{aligned}\tilde{\nu}_{ji} &= \frac{V_{ji}^2}{\hbar} \sqrt{\frac{\pi}{\lambda k_{\mathrm{B}} T}} \exp\left[-\frac{(-\vec{\mathcal{F}}\vec{r}_{ji} + \lambda)^2}{4\lambda k_{\mathrm{B}} T}\right] \\ &= \nu_{ji} \exp\left[-\frac{(\vec{\mathcal{F}}\vec{r}_{ji})^2 - 2\lambda\vec{\mathcal{F}}\vec{r}_{ji}}{4\lambda k_{\mathrm{B}} T}\right]\end{aligned} \tag{4}$$

This resembles the Marcus equation for charge transport.[31,32] $\vec{\mathcal{F}}$ is a nonphysical, fictitious "force" that accelerates the exciton to the average velocity $\langle v \rangle$:

$$\langle v \rangle = \sum_{ij} p_i \tilde{\nu}_{ji} \vec{r}_{ji} \frac{\vec{\mathcal{F}}}{\mathcal{F}} \tag{5}$$

p_i is the occupation probability of the lattice site i and can be calculated by a master equation approach.[35] (Because of the drift term in eq 4, p_i is no longer the same for all sites.) An "exciton mobility"

$$\mu = \frac{\langle v \rangle}{\mathcal{F}} \tag{6}$$

can be defined complying the Einstein relation,[57,58] which relates the mobility with the diffusion constant:

$$\frac{D}{\mu} = k_B T \tag{7}$$

If one regards the limiting case of a vanishing force $\vec{\mathcal{F}}$, the equations again become physically reasonable and the diffusion constant is calculated via

$$D = \lim_{\mathcal{F}\to 0} \frac{k_B T}{\mathcal{F}} \sum_{ij} p_i \tilde{\nu}_{ji} \left[\vec{r}_{ji} \left(\frac{\vec{\mathcal{F}}}{\mathcal{F}} \right) \right] \tag{8}$$

The diffusion length can be calculated as

$$L = \sqrt{2D\tau} \tag{9}$$

if the exciton lifetime τ is known.

It has been previously shown that the classical Einstein relation (eq 7), which states that the diffusion to drift ratio equals the thermal energy, does not hold in the presence of a drift term in the rate equation (eq 1), which is based on the spectral overlap.[25] However, it does hold when applying the Marcus theory. A Taylor approximation of eq 4 for small $\mathcal{F}$ leads to

$$\tilde{\nu}_{ji} \approx \nu_{ji} \left(1 + \frac{\vec{\mathcal{F}} \vec{r}_{ji}}{2k_B T} \right) \tag{10}$$

For simplicity, only one dimension is regarded in the following. The diffusion constant is

$$\begin{aligned} D &= \frac{1}{2} \langle \tilde{\nu}_{ji} r_{ji}^2 \rangle \\ &= \frac{1}{2} \left\langle \nu_{ji} \left(1 + \frac{\mathcal{F} r_{ji}}{2k_B T} \right) r_{ji}^2 \right\rangle \\ &= \frac{1}{2} \left(\langle \nu_{ji} r_{ji}^2 \rangle + \frac{\mathcal{F}}{2k_B T} \langle \nu_{ji} r_{ji}^3 \rangle \right) \\ &= \frac{1}{2} \langle \nu_{ji} r_{ji}^2 \rangle \end{aligned} \tag{11}$$

The second summand vanishes because $\nu_{ij} = \nu_{ji}$ and $r_{ij} = -r_{ji}$. This reveals that the diffusion is not influenced by the drift, provided that $\mathcal{F}$ is sufficiently small and nonlinear effects can be neglected. The mobility is defined as

$$\begin{aligned} \mu &= \frac{1}{\mathcal{F}} \langle \tilde{\nu}_{ji} r_{ji} \rangle \\ &= \frac{1}{\mathcal{F}} \left\langle \nu_{ji} \left(1 + \frac{\mathcal{F} r_{ji}}{2k_B T} \right) r_{ji} \right\rangle \\ &= \frac{1}{\mathcal{F}} \left(\langle \nu_{ji} r_{ji} \rangle + \frac{\mathcal{F}}{2k_B T} \langle \nu_{ji} r_{ji}^2 \rangle \right) \\ &= \frac{1}{2k_B T} \langle \nu_{ji} r_{ji}^2 \rangle \end{aligned} \tag{12}$$

Dividing eq 11 by eq 12 leads to the Einstein relation (eq 7).

Similar approaches using the Marcus theory have already been used for charge transport.[35,59,60] Since, for charges, the coupling depends on the orbital overlap, it decays exponentially with distance, so that it is sufficient to take only the target sites in the nearest neighbored unit cells into account. However, the coupling for singlet exciton transport decays only proportional to r_{ji}^{-3}. Therefore, the extrapolation scheme described in ref 25 is used to eliminate the influence of the jump radius cutoff in the numerical calculations.

2.3. Quantum Chemical Methods. The electronic coupling V_{ji} and the reorganization energy λ needed for the hopping rate (eqs 3 and 4) were determined by quantum chemical first-principles calculations. In order to calculate λ, the monomer geometry is optimized for the ground state and the excited state. The energies of the ground and excited state in their respective minimum geometries (E_g and E_{ex}, respectively), the ground-state energy of the excited-state geometry (E_g^*) and the excited-state energy of the ground state geometry (E_{ex}^*) are calculated to obtain the intramolecular (internal) reorganization energy[43,61,62]

$$\begin{aligned} \lambda &= \lambda_{ex} + \lambda_g \\ &= (E_{ex}^* - E_{ex}) + (E_g^* - E_g) \end{aligned} \tag{13}$$

(cf. Figure 1). To test the influence of the quantum chemical method on the result, we compare spin-component scaled[63,64] approximate coupled-cluster singles and doubles[65−68] (SCS-CC2), time-dependent Hartree−Fock (TDHF) and time-dependent density functional theory using the hybrid generalized gradient functional B3LYP[69−74] and the generalized

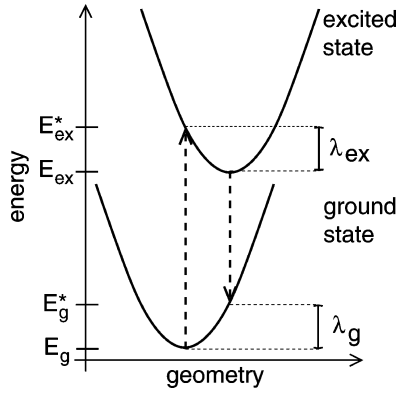

Figure 1. Depiction of the potential energy surfaces of the ground state and the excited state of the monomer. The dashed arrows indicate the vertical transitions from one state to the other. λ_g and λ_{ex} are the two contributions to the reorganization energy (see eq 13).

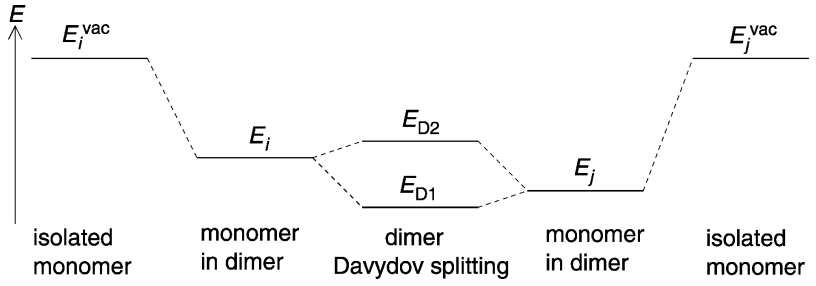

Figure 2. Depiction of the excitation energies. The excitation energies of the isolated monomers, $E_i^{vac} = E_j^{vac}$, are lowered in the presence of the other monomer to $E_i \neq E_j$. Davydov splitting leads to the dimer excitation energies E_{D1} and E_{D2}.

gradient functional BLYP,[69,70,73] together with the resolution of the identity approximation[75−77] (RI-BLYP). The respective methods are employed for both geometry and energy calculations. The correlation-consistent polarized double, triple, and quadruple ζ basis sets[78] (cc-pVDZ, cc-pVTZ, cc-pVQZ, respectively) are used for all atoms. All quantum chemical calculations are performed with the Turbomole program package.[79,80]

If the monomer is excited to a higher electronic state, the internal conversion to the lowest excited state (S_1) is ∼2 orders of magnitude faster than the exciton transfer to another molecule and 10^4 times faster than the fluorescence from S_1 to the ground state S_0,[81] which is on the order of nanoseconds. For this reason, only the S_1 state of the monomer is relevant for the exciton transport.

The exciton coupling V_{ji} is calculated by a supermolecular approach of the entire dimer.[82] The interaction between the lowest excitation of one monomer with that of another is described by the Hamilton matrix,

$$\mathbf{H} = \begin{pmatrix} E_i & V_{ji} \\ V_{ji} & E_j \end{pmatrix} \tag{14}$$

provided that the lowest monomer excitations are energetically well-separated from the monomer S_2 excitations. E_i and E_j are the excitation energies of monomers i and j, respectively. It is important to be aware that the monomer excitation energies in the dimer configuration are not the same as those for an isolated molecule, since the monomers influence each other, leading to a reduction of energy (see Figure 2). If the dimer is

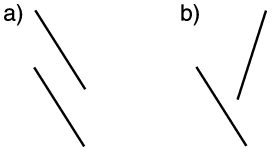

Figure 3. Graphic depiction of (a) monomers shifted in parallel, resulting in a symmetric dimer, and (b) tilted monomers, with no symmetry.

symmetric, as shown in Figure 3a, then $E_i = E_j$, and diagonalization of the Hamilton matrix **H** leads to[25,83]

$$V_{ji} = \frac{E_{D2} - E_{D1}}{2} \tag{15}$$

where E_{D1} and E_{D2} are the energies of the two lowest dimer excitations resulting from the Davydov splitting[84] of the monomer S_1 levels. However, in a crystal, many monomers are tilted with respect to each other (see Figure 3b), leading to $E_i \neq E_j$. In this case, the coupling is

$$V_{ji} = \frac{1}{2}\sqrt{(E_{D2} - E_{D1})^2 - (E_i - E_j)^2} \tag{16}$$

Yet, it will be shown in section 3 that eq 15 is a very good approximation, even for tilted monomers, and can therefore be used for all monomer arrangements in the crystal. Thermal motion of the monomers is neglected. This should be justified for excitons even more than for charge carriers, since the exciton coupling is less dependent on the distance.[25]

The simple molecular approach does not work if the energetic separation between the first and second monomer excitation is not large, compared to their energetic splitting in the dimer, because the excitations of one monomer do not only interact with their counterparts at the other monomer, but also with all others, which are energetically close. In that case, a fitting procedure as described in ref 25 can be used. For sufficiently large distances, the couplings can be approximated by the dipole interaction.[25] In order to account for the molecular screening caused by the other monomers, the coupling to the monomers beyond the directly neighboring cells is divided by the relative dielectric constant ε_r, which depends on the material and on the spatial direction in the crystal. However, it has already been shown that the anisotropy of the dielectric constant does not contribute strongly to the anisotropy of the diffusion constant in the crystal[25] and therefore can be neglected.

The quantum chemical methods which are applied to test their influence on the coupling parameter and the diffusion length are TDHF, SCS-CC2,[85] and the spin-component-scaled algebraic diagrammatic construction through second order[86] (SCS-ADC(2)), together with the cc-pVDZ, cc-pVTZ, and cc-pVQZ basis sets for all atoms. The nonvariational coupled cluster approach leads to a right and a left transition dipole moment because of the non-Hermitian Hamiltonian caused by a similarity transformation.[87] For that reason, the arithmetic mean of both vectors is used.

It has been shown, for smaller molecules, that SCS-CC2 and SCS-ADC(2) excitation energies compare quite well with full configuration interaction calculations,[88,89] whereas TDHF leads to larger errors.[88,90] CC-based methods are very accurate if the excited and ground states are mainly described by single excitations.[91] By applying spin-component scaling, the accuracy of the excitation energies further increases[64,92] without additional computational cost. SCS-CC2 delivers excellent excitation energies also for larger molecules as, for example, perylene-based dye-aggregates[93] and paracyclophanes.[94,95] It has been shown that TDHF,[83,90,96] as well as CC2 and ADC(2),[97] lead to transition dipole moments that agree well

dx.doi.org/10.1021/ct500014h | J. Chem. Theory Comput. 2014, 10, 1242−1255

with experimental values. Applying spin scaling to the latter two improves the results further.[97]

It is known that time-dependent density functional theory (TDDFT) often predicts excitation energies that are substantially too low,[98] especially for charge-transfer states,[93,99−102] leading furthermore to an erroneous influence on the neutral states, which are energetically close.[83,90] For that reason, TDDFT was not investigated in this context.

3. RESULTS AND DISCUSSION

If not otherwise stated, the cc-pVTZ basis set was used. The couplings were calculated with the SCS-ADC(2) method. Optimizations and calculations of the reorganization energies were conducted with SCS-CC2. The hopping rates were calculated at a temperature of T = 300 K and a ficticious "force" (see eq 4) of $\mathcal{F}$ = 16 aN was applied. The molecules under investigation are depicted in Figure 4, and the crystallographic parameters of the corresponding crystals are listed in Table 1.

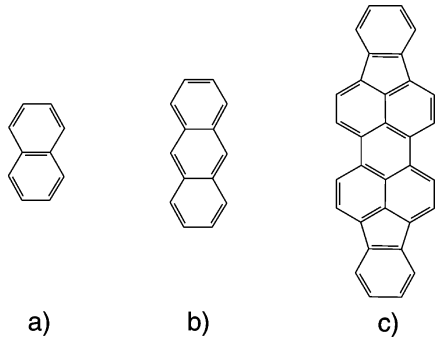

Figure 4. Sketch of the molecules investigated in this work: (a) naphthalene, (b) anthracene, and (c) diindenoperylene.

3.1. Naphthalene. The naphthalene crystal consists of two differently orientated monomers (Figure 4a) per unit cell.[103] (See Table 1 for the crystal parameters.) Table 2 shows the vertical monomer excitation energies of the two lowest excitations, 1^1B_{3u} and 1^1B_{2u}, which have a single excitation contribution of 89% and 91%, respectively. The S_1 state (called α or L_b, B_{3u} symmetry) is energetically well-separated from the S_2 state (p or B_a, B_{2u} symmetry) so that no mixing between these states has to be considered. Note that, for TDHF, the energetical order is reversed. The corresponding adiabatic excitation energies are listed in Table 3.

Table 4 shows the reorganization energy for the 1^1B_{3u} excitation of naphthalene calculated with different methods and basis sets. The influence of the basis set is negligible; however, the strong dependence on the method becomes obvious. While SCS-CC2, as the presumably most accurate method, predicts a reorganization energy of 350 meV, TDHF gives rise to a much larger value of ∼520 meV. (This is regarded in more detail for anthracene in section 3.2.1.) Both tested DFT approaches considerably underestimate the reorganization energy in comparison to SCS-CC2. Since the reorganization energy enters the hopping rate exponentially (see eqs 3 and 4), variations in the reorganization energy change the diffusion constant by almost 2 orders of magnitude, cf. Figure 5. This indicates that at least the reorganization energies have to be computed with high-level ab initio methods to achieve reliable estimates for D. However, this is feasible since λ only has to be computed once.

SCS-CC2 tends to slightly overestimate bond lengths, compared to experiments, and correspondingly underestimates the vibrational frequencies. However, since the deviations have the same sign for both the ground state and the excited state, changes in the bond length and the frequencies are obtained with quite high accuracy,[68] so that the reorganization energies obtained with SCS-CC2 seem to be reliable. TDDFT was shown to be less trustworthy than SCS-CC2.[68,108] Hartree−Fock overestimates the vibrational frequencies in the ground state.[109,110] However, it is shown in detail in section 3.2.1 that this does not hold correspondingly for excited states, which is the reason for the much-higher λ value. Furthermore, TDHF

Table 2. Vertical Excitation Energies of the Two Lowest Excitations in the Naphthalene Monomer[a]

	Vertical Excitation Energy (eV)		
state	TDHF	SCS-CC2	SCS-ADC(2)
$S_1(\alpha)1^1B_{3u}$	5.00 (5.12)	4.36 (4.46)	4.37 (4.47)
$S_2(p)1^1B_{2u}$	4.73 (4.83)	4.95 (5.04)	4.92 (5.01)

[a]The structure was optimized in the ground state with SCS-CC2/cc-pVTZ. The values for the non-optimized monomer structure taken from the X-ray crystal data are given in brackets.

Table 3. Adiabatic Excitation Energies of the Two Lowest Excitations in the Naphthalene Monomer[a]

	Adiabatic Excitation Energy (eV)			
state	TDHF	SCS-CC2	experiment	ref source(s)
$S_1(\alpha)1^1B_{3u}$	4.94	4.18	3.97	105
			4.0	106
$S_2(p)1^1B_{2u}$	4.53	4.62	4.45	105, 106
			4.7	107

[a]Both geometry optimization and energy calculations were conducted with the same respective method and the cc-pVTZ basis set. (Note that the calculated values do not include a zero-point correction.)

Table 4. Reorganization Energy of Naphthalene Calculated with Different Methods and Basis Sets

	Reorganization Energy (meV)		
	cc-pVDZ	cc-pVTZ	cc-pVQZ
RI-BLYP	183	187	186
B3LYP	213	218	216
TDHF	515	527	525
SCS-CC2	351	347	345

Table 1. Lattice Constants and Angles for the Unit Cells of All Calculated Crystals

	a [nm]	b [nm]	c [nm]	α [deg]	β [deg]	γ [deg]	ref
naphthalene	0.869	0.601	0.829	90.00	122.60	90.00	103
anthracene	0.850	0.600	1.114	90.00	124.91	90.00	104
diindenoperylene	0.717	0.855	1.680	90.00	92.42	90.00	36

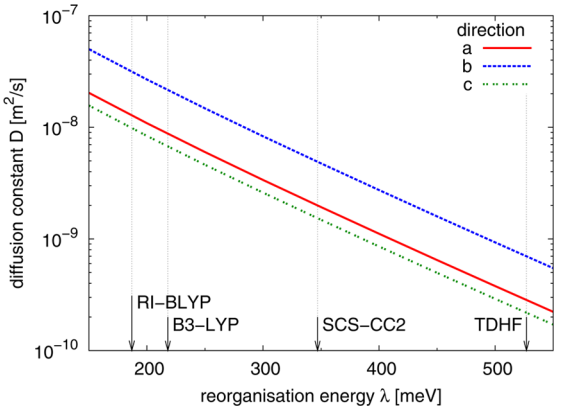

Figure 5. Plot showing the diffusion constant (D) of naphthalene along the unit-cell vectors, depending on the reorganization energy (λ). The λ values from Table 4 are tagged by arrows. (V_{ji} was calculated with SCS-ADC(2)/cc-pVTZ.)

does not include electron correlation and is therefore inferior to SCS-CC2 and SCS-ADC(2).

Table 5 shows the largest coupling in the naphthalene crystal, which is the coupling between the two monomers in the same unit cell. Obviously, the basis sets do not have much influence and even the methods do not differ significantly in this case.

Table 5. Largest Coupling (V_{ji}) in the Naphthalene Crystal, Which is the Coupling between the Two Monomers in the Unit Cell

	Largest Coupling, V_{ji} (meV)		
	cc-pVDZ	cc-pVTZ	cc-pVQZ
TDHF	9.3	9.5	9.5
SCS-CC2	7.5	7.4	7.5
SCS-ADC(2)	6.8	7.1	7.1

Because of the small transition dipole moment of the 1^1B_{3u} excitation,[111,112] the couplings are rather low. Beyond a monomer distance of 1 nm, the couplings calculated with the supermolecular approach (eq 15) do not differ strongly from those calculated with the dipole approximation.[25] For that reason, the supermolecular approach was used up to a distance of 1.5 nm; beyond that distance, the dipole approximation was used. Because of the small couplings, the dielectric shielding (ε_r = 2.5; see ref 113) does not influence the diffusion constant.[25] For the same reason, it was not necessary to extrapolate D for an infinite jump radius, as mentioned in section 2.2; instead, a fixed maximum jump radius of 2.5 nm turned out to be adequate.

Table 6 shows exciton diffusion constants as obtained with the coupling parameters V_{ji} from the different quantum chemical methods and basis sets. The reorganization energy (λ) was set to 347 meV (SCS-CC2, cc-pVTZ) in order to identify the influence of the coupling calculations. It can be seen that TDHF overestimates the diffusion constant, compared to the higher level methods SCS-CC2 and SCS-ADC(2). Since the coupling enters the hopping rate quadratically (cf. eqs 3 and 4), the differences between the methods used for the couplings have a stronger influence on the diffusion constants than on the couplings themselves. In this context, the trend of D, depending on the basis set, is not yet clear, because it behaves differently for the different directions. We assume, as a possible reason, that the couplings in the naphthalene crystal are quite small, so that the inaccuracies of the methods become more important than the influence of the basis sets.

Table 6. Exciton Diffusion Coefficient (D) in the Naphthalene Crystal, Depending on the Method and the Basis Sets Used for the Couplings[a]

	Exciton Diffusion Coefficient ($\times 10^{-9}$ m^2/s)		
	cc-pVDZ	cc-pVTZ	cc-pVQZ
	***a*-direction**		
TDHF	5.1	3.0	2.3
SCS-CC2	1.4	2.1	
SCS-ADC(2)	3.0	2.0	
	***b*-direction**		
TDHF	8.9	9.0	8.8
SCS-CC2	5.3	5.3	
SCS-ADC(2)	4.8	4.9	
	***c*-direction**		
TDHF	3.6	4.0	4.3
SCS-CC2	1.4	1.5	
SCS-ADC(2)	1.7	1.5	

[a]The reorganization energy was λ = 347 meV (SCS-CC2/cc-pVTZ) for all calculations.

In order to compare the differences for the different quantum chemical methods used for the coupling, Figure 6 shows the diffusion length L in the (ab) plane, assuming an exciton lifetime of 78 ns.[114−116] The reorganization energy is λ = 347 meV (SCS-CC2/cc-pVTZ) for all calculations. As already seen in Table 6, SCS-CC2 and SCS-ADC(2) lead to similar results, while TDHF leads to larger diffusion lengths.

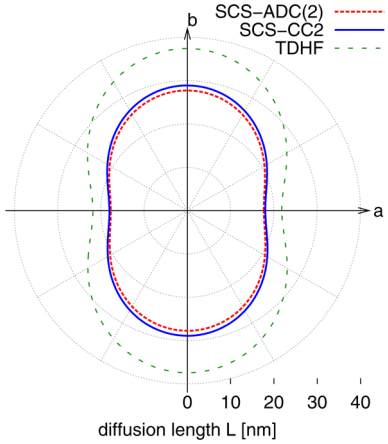

Figure 6. Exciton diffusion length in the naphthalene crystal in the (ab) plane (τ = 78 ns; see refs 114−116). The couplings were calculated with SCS-ADC(2), SCS-CC2, and TDHF, respectively. In all cases, the cc-pVTZ basis sets were used, and the reorganization energy was calculated with SCS-CC2/cc-pVTZ.

Table 7 shows a comparison of the exciton diffusion constants and lengths between those obtained with the Marcus theory, an approach using eq 1 as described in ref 25, and experimental values. While the values calculated with eq 1 fit very accurately to the measurements, the Marcus theory yields smaller values. The FCWD (eq 2) for naphthalene is J = 0.71 eV^{-1} (from ref 25, calculated with SCS-CC2, cc-pVTZ). The corresponding value in the Marcus theory,

Table 7. Exciton Diffusion Constants (D) and Diffusion Lengths (L) for Naphthalene[a]

	Diffusion Constant D ($\times 10^{-9}$ m^2/s)		
	Marcus theory	overlap[b]	measured[c]
a	2.0	14.4	
b	4.9	33.6	
c	1.5	10.3	
c'	1.3	9.0	5
	Diffusion Length L (nm)		
	Marcus theory	overlap[b]	measured[d]
a	18	48	50[e]
b	28	72	
c	15	40	
c'	14	37	

[a]V_{ji} was calculated with SCS-ADC(2)/cc-pVTZ, λ was calculated with SCS-CC2/cc-pVTZ. [b]Data taken from ref 25. [c]Data taken from ref 117. [d]Data taken from ref 116. [e]Direction unknown.

$$J_{\text{Marcus}} = \frac{1}{2\sqrt{\pi\lambda k_B T}} \exp\left(-\frac{\lambda}{4k_B T}\right) \quad (17)$$

is 0.10 eV^{-1} (with λ = 347 meV, also calculated with SCS-CC2, cc-pVTZ). J_{Marcus} is smaller than J because, in the Marcus theory, a quasi-classical approximation is employed which underestimates the delocalization of the nuclear positions. This corresponds to narrow absorption and emission spectra, resulting in a smaller overlap of the spectra. Therefore, the diffusion constants calculated with the more-precise eq 1 are larger by a factor of 6.9, while the diffusion lengths are bigger by a factor of 2.6. Figure 7 compares both approaches and Monte Carlo simulations using Marcus theory to verify our approach for the transport calculations, as explained in section 2.2 within the three principal crystal planes.

3.2. Anthracene. The anthracene lattice parameters are listed in Table 1. The unit cell contains two differently oriented monomers.[104] The monomer is depicted in Figure 4b. Table 8 lists the adiabatic excitation energies of the first two monomer excitations, which have B_{2u} (S_1) and B_{3u} (S_2) symmetry, respectively, with single excitation contributions of 89% and 91%. The vertical excitation energies are shown in Table 9. Compared to naphthalene, the 1^1B_{2u} and 1^1B_{3u} symmetries are energetically interchanged[111,112] and in close proximity. (Also compare the experimental values in Table 8.) For SCS-CC2 and SCS-ADC(2), the 1^1B_{2u} and 1^1B_{3u} vertical excitation energies even change order, although the order of the adiabatic excitation energies is correctly reproduced.

Table 8. Adiabatic Excitation Energies of the Two Lowest Excitations in the Anthracene Monomer[a]

	Adiabatic Excitation Energy (eV)			
state	TDHF	SCS-CC2	experiment	ref source
$S_1(p)$ 1^1B_{2u}	3.57	3.56	3.31	111
			3.43	118
$S_2(\alpha)$ 1^1B_{3u}	4.36	3.69	3.45	119
			3.84	120

[a]Both geometry optimization and energy calculations were conducted with the same respective method and cc-pVTZ. (The calculated values are without zero point correction.)

Table 9. Vertical Excitation Energies of the Two Lowest Excitations in the Anthracene Monomer Calculated with Different Methods and the cc-pVTZ Basis Set[a]

	Vertical Excitation Energy (eV)		
state	TDHF	SCS-CC2	SCS-ADC(2)
$S_1(p)1^1B_{2u}$	3.70 (3.82)	3.84 (3.94)	3.83 (3.91)
$S_2(\alpha)1^1B_{3u}$	4.37 (4.43)	3.82 (3.89)	3.81 (3.89)

[a]The structure was optimized in the ground state with SCS-CC2/cc-pVTZ. The value for the non-optimized monomer structure as taken from the X-ray crystal data are given in brackets.

Table 10 shows the reorganization energy of anthracene calculated with different methods and basis sets. Although λ increases by ~5% going from a double-ζ basis set to a triple-ζ basis set, the change from triple-ζ to quadruple-ζ is very small (~2% variation) and lies in the range of the accuracy of the method. It seems that the energy is already converged for the

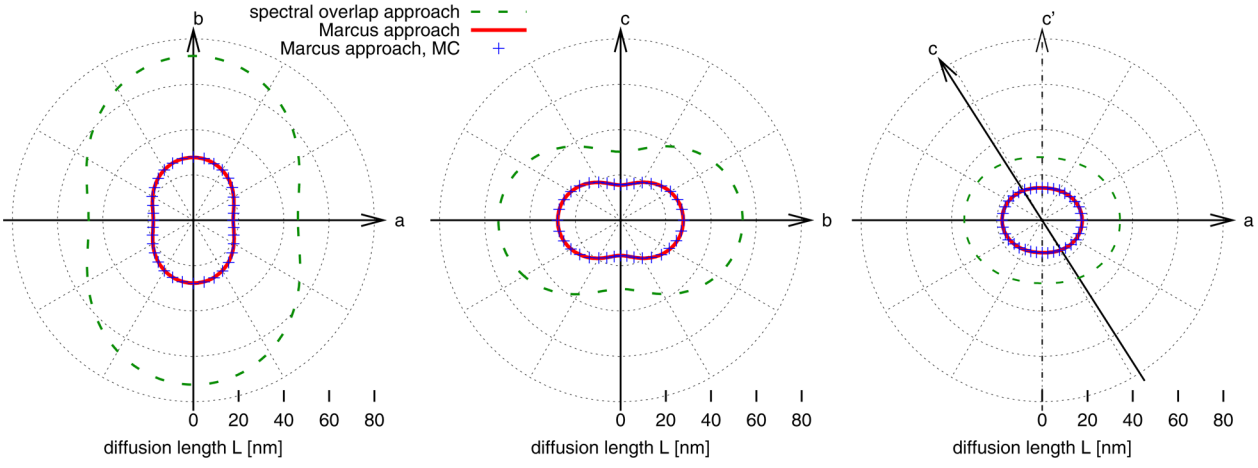

Figure 7. Exciton diffusion length in the naphthalene crystal in the (ab) plane (left), (bc) plane (middle), and (ac) plane (right). The green dashed lines were calculated with the spectral overlap approach using eq 1, as explained in ref 25, the red solid lines were calculated with the Marcus equation (eqs 4 and 8), along with the master equation and the blue crosses were calculated with the Marcus equation (eq 3), using the Monte Carlo method. (V_{ji} was calculated with SCS-ADC(2), cc-pVTZ, λ, and J were calculated with SCS-CC2, cc-pVTZ.)

Table 10. Reorganization Energy of Anthracene Calculated with Different Methods and Basis Sets

	Reorganization Energy (meV)		
	cc-pVDZ	cc-pVTZ	cc-pVQZ
RI-BLYP	323	341	340
B3-LYP	423	445	444
TDHF	876	921	923
SCS-CC2	509	530	533

cc-pVTZ basis set and, for that reason, it was used for all further calculations.

As already seen for naphthalene, there are severe differences for λ, depending on the quantum chemical method used. TDDFT leads to the lowest energies, while TDHF highly overestimates the reorganization energies. Because of the exponential dependency of the jump rate on λ (eqs 3 and 4), the diffusion constant changes even by 3 orders of magnitude depending on the method used (see Figure 8).

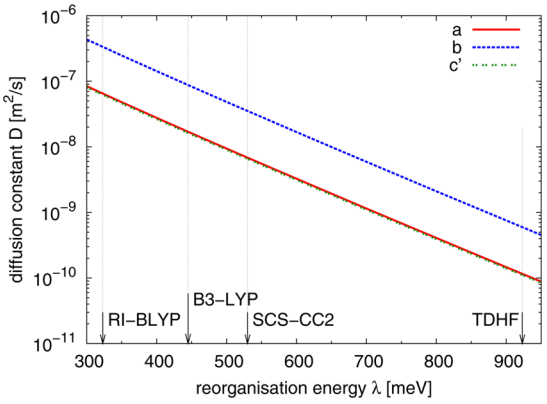

Figure 8. Diffusion constant of anthracene along the unit-cell vectors, depending on the reorganization energy λ. The λ values from Table 10 are tagged by arrows. (V_{ji} was calculated with SCS-ADC(2), cc-pVTZ.)

The reorganization energy calculated with TDHF is about a factor of 1.74 larger than the more-reliable energy calculated with SCS-CC2 (both with cc-pVTZ). This is caused by the larger geometry change for TDHF due to the excitation, as will be explained in section 3.2.1.

Since the first two excitations in the anthracene monomer are energetically very close (see Tables 8 and 9), they do not only interact with their respective counterparts of the other monomer; instead, these two excited monomer states mix if the resulting dimer is not symmetric[25] as, e.g., the dimer depicted in Figure 9a, which is the dimer consisting of the two monomers in the unit cell. For that reason, eqs 15 and 16 cannot be used to calculate the coupling. Instead, a fitting procedure such as that described in ref 25 can be used.

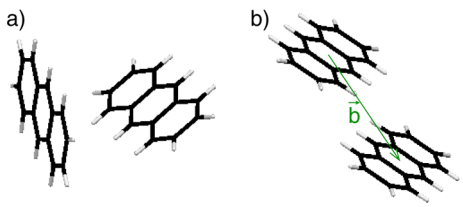

Figure 9. Two dimers in the anthracene crystal: (a) dimer in the unit cell and (b) dimer with the highest coupling (monomers shifted by the lattice vector $\vec{b}$).

Figure 9b shows the dimer with the highest coupling in the anthracene crystal. Here, one monomer is shifted parallel by the lattice vector $\vec{b}$, relative to the other. Because of the dimer symmetry, the 1^1B_{2u} and 1^1B_{3u} monomer excitations do not mix and eq 15 can be applied in this case. Table 11 shows the coupling of this dimer calculated via both the supermolecular approach and the dipole approximation with different quantum chemical methods and basis sets. As for the reorganization energy, the dependency on the basis set is not very strong; however, the coupling decreases slightly as the basis set increases. More important is the dependency on the method used. While SCS-CC2 and SCS-ADC(2) lead to similar values, the coupling calculated with TDHF is a factor of ∼1.5 larger. For SCS-CC2 and SCS-ADC(2), the accordance between the dipole approximation and the supermolecular approach increases with increasing basis set, whereas, for TDHF, depending on the basis set, no improvement is observed. The best agreement between the supermolecular calculation and the dipole approximation is found for SCS-ADC(2), which is also the most reliable approach for the present problem, because it is accounting for electron correlation and applicable to almost-degenerate cases. Thus, SCS-ADC(2) is mostly used in this paper. In order to avoid the quite laborious supermolecular fitting procedure, the dipole approximation was used for all couplings in the anthracene crystal.

Table 11. Largest Coupling in the Anthracene Crystal (V_{ji}), Calculated with Different Quantum Chemical Methods and with Both the Supermolecular Approach and the Dipole Approximation (the Corresponding Dimer is Depicted in Figure 9b)

	Largest Coupling, V_{ji} (meV)		
	cc-pVDZ	cc-pVTZ	cc-pVQZ
supermolecular, TDHF	39.82	37.22	36.31
supermolecular, SCS-CC2	25.62	23.08	21.37
supermolecular, SCS-ADC(2)	25.26	24.17	23.38
dipole approx., TDHF	29.92	27.36	26.34
dipole approx., SCS-CC2	22.02	20.38	19.67
dipole approx., SCS-ADC(2)	26.05	24.41	23.30

Since the anisotropy of the dielectric constant is not important for the anisotropy of the exciton transport,[25] a value of $\varepsilon_r = 3$ was used for all calculations. In Table 12, the diffusion constants in different directions, which were calculated with different quantum chemical methods and basis sets, are listed. As for the coupling (see Table 11), D slightly decreases as the basis set increases. From the quadruple-ζ basis set to the smaller triple-ζ basis set, D increases by ∼8% on average; from triple-ζ to double-ζ, it increases ∼14%. The triple-ζ basis set seems to be a good compromise, particularly since quadruple-ζ basis sets are often too big for calculations of typical organic molecules, which are used for semiconductor application. As already seen in the case of the couplings (Table 11), the diffusion constant is considerably dependent on the quantum chemical method used. TDHF overestimates D, compared to the higher-level methods SCS-CC2 and SCS-ADC(2). The values calculated with TDHF are a factor of ∼1.8 larger than the values determined with SCS-CC2. However, the SCS-CC2 values are a factor of ∼0.7 smaller than the SCS-ADC(2) values. As already seen in Table 11, the supermolecular

dx.doi.org/10.1021/ct500014h | J. Chem. Theory Comput. 2014, 10, 1242−1255

Table 12. Exciton Diffusion Coefficients in the Anthracene Crystal, Depending on the Method and the Basis Sets Used for the Couplings (ε = 3)[a]

	Exciton Diffusion Coefficient ($\times 10^{-9}$ m^2/s)		
	cc-pVDZ	cc-pVTZ	cc-pVQZ
	***a*-direction**		
TDHF	10.5	8.8	8.2
SCS-CC2	5.6	4.8	4.5
SCS-ADC(2)	7.9	6.9	6.1
	***b*-direction**		
TDHF	53.3	44.7	41.4
SCS-CC2	28.8	24.7	23.0
SCS-ADC(2)	40.3	35.3	32.1
	***c*-direction**		
TDHF	10.3	8.7	8.1
SCS-CC2	5.5	4.8	4.4
SCS-ADC(2)	7.8	6.8	6.0
	***c*′-direction**		
TDHF	10.1	8.5	7.9
SCS-CC2	5.4	4.6	4.3
SCS-ADC(2)	7.6	6.6	5.9

[a]The reorganization energy was λ = 530 meV (SCS-CC2/cc-pVTZ) for all calculations.

approach leads to quite similar results for the coupling for SCS-ADC(2) and SCS-CC2; however, the dipole approximation is better for SCS-ADC(2). This seems to be the reason for the deviations between both methods in the calculation of D.

Experimental estimations of the diffusion constants have led to values of $D \leq 5 \times 10^{-8}$ m^2/s in the b-direction and $D \leq 10^{-8}$ m^2/s in the c-direction.[121] This fits quite well with the calculated results of 3.5×10^{-8} m^2/s for the b-axis and 0.7×10^{-8} m^2/s for the c-axis.

Table 13 shows a comparison of the calculated diffusion lengths with experimental values[122,123] and with values calculated with eq 1 and the approach described in ref 25. The FCWD (eq 2) for anthracene is J = 0.35 eV^{-1} [25] (calculated with SCS-CC2, cc-pVTZ) while the corresponding expression in the Marcus theory (eq 17) has a value of 0.01 eV^{-1} (λ = 530 meV, calculated with SCS-CC2, cc-pVTZ).

Table 13. Comparison of Diffusion Lengths for Anthracene (τ = 10 ns; see refs 116, 124, and 125) Calculated with the Marcus Theory, the Spectral Overlap Approach (eq 1), and Experimental Values[a]

	Diffusion Length			
	Marcus theory	overlap[b]	measured	ref source
a-direction	12	58	60 ± 10	122
b-direction	27	132	∼100	122
c-direction	12	58		
c′-direction	11	57	60 ± 5	123
			49 ± 1	127
			47 ± 1	127
			36 ± 20	122

[a]Note that the measured values have not been corrected for reabsorption. V_{ji} was calculated with SCS-ADC(2), cc-pVTZ, λ was calculated with SCS-CC2, cc-pVTZ. [b]Data taken from ref 25.

Therefore, the diffusion constants determined with eq 1 are larger, by a factor of 24.7, while the diffusion lengths differ by a factor of 5.0.

For the calculation of L, an exciton lifetime of 10 ns was assumed.[116,124,125] There are also higher values found in the literature,[114,115,126] but it seems that these values have not been corrected for the reabsorption effect.[125] In the anthracene crystal, the absorption and emission spectra overlap, leading to the effect that an emitted photon is absorbed again at another crystal site. The calculated results compare qualitatively well with the experimental values. As in the experiment, the b-direction is the one with the highest diffusion length, and this value is about twice as large as in the a- and c′-directions. The calculated diffusion lengths are smaller than the corresponding measured ones and those calculated with the approach using eq 1,[25] depending on the direction, by a factor of ∼4−5. Figure 10 depicts the diffusion lengths along all spatial directions.

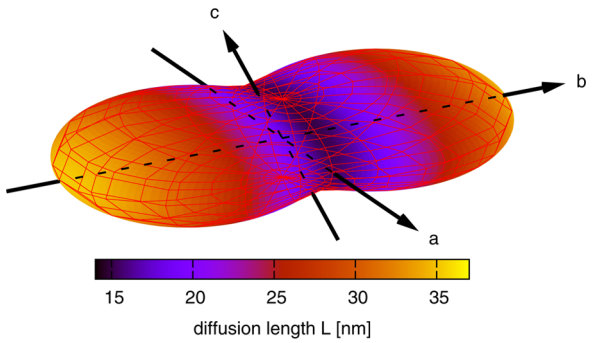

Figure 10. Exciton diffusion length in the anthracene crystal along all spatial directions. (V_{ji} was calculated with SCS-ADC(2)/cc-pVTZ, and λ was calculated with SCS-CC2/cc-pVTZ.)

3.2.1. Comparison of the Reorganization Energies Calculated with TDHF and SCS-CC2. In order to have a closer look at the large differences between the reorganization energies calculated with TDHF and SCS-CC2, the difference vectors of the atomic positions of the excited-state and the ground-state structure were calculated for both TDHF ($\vec{R}_{TDHF}$) and SCS-CC2 ($\vec{R}_{CC2}$). The angle between these two vectors is 14°, which means that the vectors can be regarded as almost parallel and the relaxation can be described as a one-dimensional motion in a harmonic potential with the energy

$$E = \frac{1}{2}KR^2 \tag{18}$$

where R is the coordinate characterizing the geometry and K is the force constant. Multiples x of the average shift vector $\vec{R} = 0.5(\vec{R}_{TDHF} + \vec{R}_{CC2})$ are added to the respective TDHF and SCS-CC2 ground-state structures and the excited-state energies for these geometries are calculated, leading to the parabolas in Figure 11. Fitting these parabolas leads to x_{TDHF} = 1.14 and x_{CC2} = 0.85 for the minima, which correspond to the excited-state geometries. The fitted curvatures are K_{TDHF} = 0.68 eV and K_{CC2} = 0.76 eV. This is quite surprising, because, for ground-state vibrations, it has been shown that the overestimation of the force constant is stronger for Hartree−Fock (6%)[109,110] than for second-order Møller−Plesset perturbation theory (MP2, 3%),[109] which is very similar to CC2 for ground-state calculations. However, here, excited-state vibrations also are involved, making the situation more complex. A rough estimation leads to

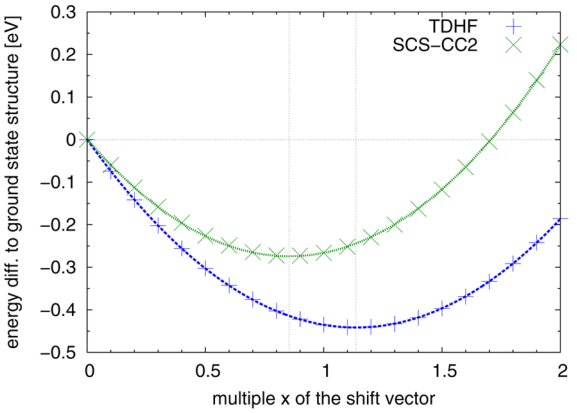

Figure 11. Excited-state energy for different structures, depending on the multiple x of the shift vector $\vec{R}$. The zero point is the ground-state structure of TDHF and SCS-CC2, respectively, and their respective excited-state energies. The dashed lines indicate the energy minima of the parabolas, corresponding to the respective excited-state geometries.

$$\frac{E_{\mathrm{TDHF}}}{E_{\mathrm{CC2}}} = \frac{0.68}{0.76}\left(\frac{1.14}{0.85}\right)^2 = 1.61 \tag{19}$$

which is quite close to the actual value of 1.74. This calculation shows that the reason for the quite large reorganization energy for TDHF (see Table 10) is caused essentially by the larger geometry change due to the excitation.

3.3. Diindenoperylene. Because of the size of the diindenoperylene molecule (Figure 4c), all calculations were conducted with the cc-pVDZ basis sets. This seems to be sufficiently accurate, since, as shown for naphthalene and anthracene, the couplings and reorganization energies are only slightly affected by the basis sets (cf. Tables 4, 5, 11, and 10).

It has been shown that, above 80 K, the exciton transport in diindenoperylene is incoherent with activation energies of 10–20 meV.[24] This legitimates the hopping approach. Table 14 lists the three lowest excitations in the diindenoperylene monomer. The excitations are sufficiently separated so that no mixing of the states can occur. Excitation of the ground state to the lowest excited state (1^1B_{3u}) gives rise to a very large oscillator strength, while the second excitation (1^1B_{1g}) is dipole-forbidden. The third excitation (1^1B_{2u}, 3.5 eV) is dipole-allowed; however, the oscillator strength is virtually zero. The transition density of the first monomer excitation is depicted in Figure 12a. The transition dipole moment is parallel to the long axis of the molecule, as indicated by the arrow. Figure 12b shows the transition density of the first two excitations of the dimer in the unit cell. These excitations are minus and plus linear combinations of the 1^1B_{3u} monomer excitations and, therefore, the supermolecular approach can be applied.

Table 14. Vertical Excitation Energies, Oscillator Strengths, and the Fractions of Single Excitations of the Three Lowest Excitations in the Diindenoperylene Monomer[a]

state	vertical excitation energy, E_{ex} [eV]	oscillator strength, f_{osc}	contrib. single excitation [%]
$S_1 1^1B_{3u}$	2.75 (2.90)	1.050 (1.054)	90 (90)
$S_2 1^1B_{1g}$	2.92 (3.12)	0.000 (0.000)	90 (90)
$S_3 1^1B_{2u}$	3.51 (3.68)	0.002 (0.000)	90 (89)

[a]The structure was optimized with SCS-CC2/cc-pVDZ and E_{ex} and f_{osc} were calculated with SCS-ADC(2)/cc-pVDZ. The values in brackets are for the non-optimized monomer structure as it is found in the crystal structure.

Figure 13 shows the difference of the coupling V_{ji} calculated with the supermolecular approach (eq 15) and the dipole approximation, depending on the distance of the monomers. No dielectric shielding was taken into account here. For small distances, the dipole approximation leads to a large overestimation of the coupling, as expected for an H aggregate (cf. Figure 12b). For distances larger than 1.5 nm, the approximation leads to quite similar results as the supermolecular approach. In order to be safe, the couplings up to a monomer distance of 2 nm were calculated with the supermolecular approach while the dipole approximation was used for distances beyond that.

One of the dimers with the largest coupling is the one that consists of the two monomers in the unit cell (see Figure 12b). Here, the monomers are tilted, with respect to each other, as depicted in Figure 3b. As explained in detail in section 2.3, eq 15 should not be valid in this case, because both monomers have different "environments" caused by the respective other monomer, resulting in different monomer excitation energies (cf. Figure 2). In this case, eq 16 should be used. The energy of the first excitation of an isolated monomer is E^{vac} = 2.902 eV. In order to determine the monomer excitation energies in the presence of the other monomer, the fit protocol that was applied to anthracene and described in ref 25 was adapted to this two-state problem, leading to E_i = 2.859 eV and E_j = 2.841 eV. These values seem to be reasonable, because they lie approximately in the middle of the first two dimer excitations with the energies of E_{D1} = 2.776 eV and E_{D2} = 2.925 eV. The monomer excitations are reduced by 43 and 61 meV, relative to the isolated monomer, respectively, differing by 18 meV. Equation 15 leads to a coupling of V_{ji} = 74.43 meV, while eq 16 results in 73.95 meV, which is consistent with the fitted value. Therefore, it is possible to use the approximated version of eq 15 for all dimers in the crystal. However, the deviation of eq 15 from eq 16 could be stronger in the case that the transition dipole moments are aligned orthogonal, rather than almost parallel (see Figure 12b). Such dimers become important in organic crystals with an in-plane herringbone structure if the transition dipole moment lies in the direction of the short molecular axis.

For the transport calculations, a dielectric constant of ε = 7 was assumed.[128] While the dipole-allowed B_{3u} excitation has the smallest vertical excitation energy, the adiabatic B_{1g} excitation energy is 66 meV below the corresponding B_{3u} value, cf. Table 15, because the states change their energetic order during the relaxation into the equilibrium structure. In Figure 14, the parabolas of the ground state and the two excited states were determined with an analogous process, as described in section 3.2.1. Because of the small energetic gap between the two excited states, both must be taken into account for transport. Since it is assumed that the relaxation into thermal equilibrium is fast, compared to the transport (see section 2.1), the states are populated according to a Boltzmann distribution, leading to 92% of the excitons in the B_{1g} state and 8% in the B_{3u} state. However, the diffusion constant of the dipole-forbidden B_{1g} state—using the reorganization energy of 673 meV, which follows from the process where the exciton is first excited into the B_{3u} state (Figure 14)—is ∼7 orders of magnitude smaller than the diffusion constant of the B_{3u} state (λ = 361 meV, both reorganization energies calculated with SCS-CC2, cc-pVDZ).

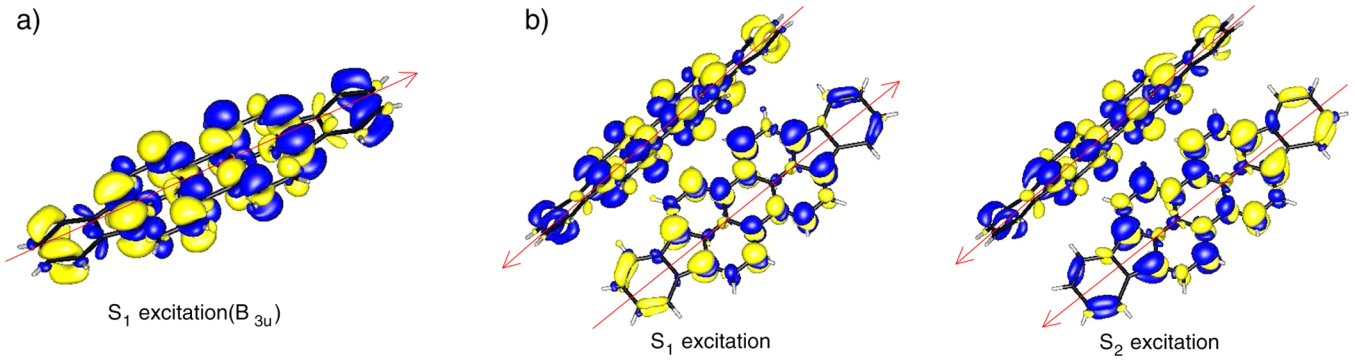

Figure 12. Graphic depictions of the transition densities of diindenoperylene: (a) the first excitation of the monomer and (b) the first two excitations of the dimer in the unit cell. (The arrows are in the direction of the transition dipole moments.)

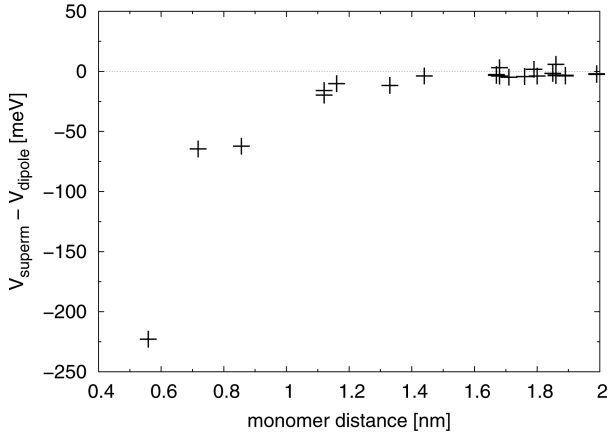

Figure 13. Difference between the electronic coupling V_{ji} for diindenoperylene calculated with the supermolecular approach and with the dipole approximation, depending on the monomer distance. (V_{ji} was calculated with SCS-ADC(2)/cc-pVDZ, and λ was calculated with SCS-CC2/cc-pVDZ.)

Table 15. Vertical and Adiabatic Excitation Energies of the Two Lowest Excitations in the Diindenoperylene Monomer[a]

state	E_{vert} [eV]	E_{adiab} [eV]
$S_1 1^1B_{3u}$	2.76	2.57
$S_2 1^1B_{1g}$	2.90	2.51

[a]Both geometry optimizations and energy calculations were conducted with SCS-CC2, cc-pVDZ. (The calculated values are without zero point correction.)

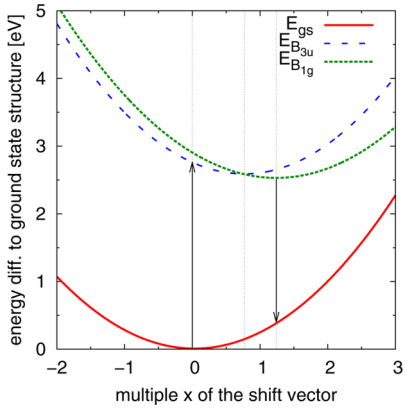

Figure 14. Energies of the ground state and the 1^1B_{3u} and 1^1B_{1g} excited states of diindenoperylene, depending on the multiple x of the shift vector $\vec{R}$, relative to the energy of the ground state in the equilibrium structure (SCS-CC2, cc-pVDZ). The dashed lines indicate the equilibrium structures.

Table 16. Diffusion Lengths for Diindenoperylene along Different Crystal Directions, Calculated with τ = 10 ns (ref 39) and with 92% B_{1g} and 8% B_{3u} Occupation[a]

	Diffusion Length (nm)		
	calculated	measured	ref source
a	75		
b	77		
c′	103	>100	39
		90	24

[a]V_{ji} was calculated with SCS-ADC(2)/cc-pVDZ, λ was calculated with SCS-CC2/cc-pVDZ.

In the *c*′-direction, the diffusion constant of B_{3u} is 6.6×10^{-6} m^2/s, and averaging over both states results in $D = 5.3 \times 10^{-7}$ m^2/s. With an exciton lifetime of 10 ns,[39] this leads to a diffusion length of 103 nm. This fits quite nicely with the measured values of $D = 5 \times 10^{-7}$ m^2/s and $L > 100$ nm[39] and $L = 90$ nm,[24] respectively. It is important to note that grain boundaries limit the exciton diffusion in diindenoperylene to ∼100 nm,[24] i.e., also for diindenoperylene, the Marcus-based values seem to underestimate the exciton diffusion lengths for a crystal without any defects, which is assumed in our modeling. Further investigations about the influence of such trapping effects are underway. Table 16 also lists the calculated diffusion lengths in the other directions. The diffusion lengths in all directions are depicted in Figure 15. As can be seen the anisotropy is less pronounced than for naphthalene and anthracene, rendering diindenoperylene interesting for application in opto-electronic devices.

4. SUMMARY AND CONCLUSIONS

The Marcus theory, which is widely used for charge transport in organic semiconductors, was transferred to exciton transport. This allows efficient calculation of exciton diffusion coefficients with first-principles methods avoiding the demanding calculation of the spectral overlap as in the commonly used equation 1 and without the need of any fitting to experimental data.

It was shown that the calculations are not very sensitive to the basis set sizes. Triple-ζ basis sets are a good compromise

dx.doi.org/10.1021/ct500014h | J. Chem. Theory Comput. 2014, 10, 1242−1255

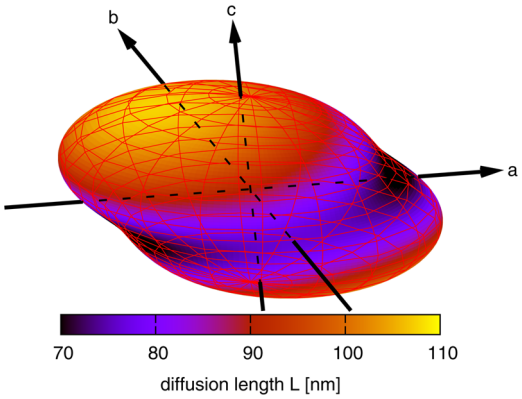

Figure 15. Exciton diffusion length in the diindenoperylene crystal in all spatial directions, calculated with a maximum jump distance of 3 nm. (V_{ji} was calculated with SCS-ADC(2)/cc-pVDZ, and λ was calculated with SCS-CC2/cc-pVDZ.)

between accuracy and computational cost, but also double-ζ basis sets lead to good results, which is important for larger molecules.

The choice of the quantum mechanical method applied has a larger effect on the predicted exciton diffusion coefficient. It was shown that TDHF overestimates the coupling compared to better methods such as SCS-CC2 and SCS-ADC(2).

Whereas the electronic coupling enters the hopping rate and, therefore, the diffusion constant quadratically, the reorganization energy enters exponentially and therefore has a large influence on D. The calculated reorganization energy (λ) is strongly dependent on the method that is employed. The simplest approach, TDHF, substantially overestimates λ, because of the strong geometry change during excitation. In comparison to the more-accurate SCS-CC2 approach, DFT approaches, on the other hand, result in much lower energies. It was shown that, in the range in which the reorganization energy varies, depending on the quantum chemical method applied, the diffusion constant varies more than 2−3 orders of magnitude. However, since it is known that SCS-CC2 leads to more-accurate energies[64,67] and because of the high influence of λ on the diffusion coefficient, it is essential to choose a preferably precise method. However, this hardly restricts the applicability of this approach, since the reorganization energy has to be calculated only for one monomer in the crystal.

The angular dependence of exciton diffusion in naphthalene, anthracene and diindenoperylene was calculated and compared with experimental findings and with calculated values obtained with the physically more-sophisticated approach containing the spectral overlap (eq 1), which is well-established for exciton transport. It was shown that the qualitative agreement is good; however, the values calculated with Marcus hopping rates tend to be considerably smaller than the measured ones, as well as those obtained with the spectral overlap approach, probably because, in the Marcus theory, only one effective vibrational mode is taken into account. Nevertheless, the Marcus-based approach seems to be sufficiently accurate to study trends. This is especially true for systems in which uncertainties in the geometrical arrangement of the monomers already may lead to error, e.g., amorphous or strongly disordered systems. The underestimation of the Marcus approach seems to be a quite general observation, since an independent study performed by Lunkenheimer and Köhn, shown at the recent symposium on Theoretical Chemistry in Erlangen,[129] came to a similar conclusion for aluminum-tris(8-hydroxy-quinoline), i.e., a completely different compound class. The anisotropy for exciton transport is less pronounced than for charge transport,[35] because the exciton couplings decay slower with distance than the charge couplings, leading to more dimers involved in the transport.

Comparing exciton and charge transport, the accordance of the Marcus-based approach with the experiment is better for exciton transport than for charge transport,[35] since, in the former case, the reorganization energy is larger and the coupling is smaller, making perturbation theory more warrantable. Furthermore, the neglected external reorganization energy should be considerably smaller for excitons than for charge carriers since excitons are neutral, therefore leading to much weaker polarization effects in the environment.

AUTHOR INFORMATION

Corresponding Author

*E-mail: Stehr@Physik.Uni-Wuerzburg.de.

Notes

The authors declare no competing financial interest.

ACKNOWLEDGMENTS

We thank BASF Ludwigshafen, Germany, for financial support and Jan Schöneboom, Christian Lennartz, and Peter Erk (BASF), for suggesting the use of Marcus theory for exciton transfer and for enlightening discussions. Financial support by the Elitenetzwerk Bayern, the Volkswagen Stiftung and the Deutsche Forschungsgemeinschaft (DFG) within the framework of the Research Training School GRK 1221 and the Research Unit 1809 is gratefully acknowledged.

REFERENCES

(1) Armstrong, N. R.; Wang, W.; Alloway, D. M.; Placencia, D.; Ratcliff, E.; Brumbach, M. *Macromol. Rapid Commun.* **2009**, *30*, 717−731.
(2) Meerheim, R.; Luessem, B.; Leo, K. *Proc. IEEE* **2009**, *97*, 1606−1626.
(3) Kulkarni, A. P.; Tonzola, C. J.; Babel, A.; Jenekhe, S. A. *Chem. Mater.* **2004**, *16*, 4556−4573.
(4) Dimitrakopoulos, C.; Malenfant, P. *Adv. Mater.* **2002**, *14*, 99−117.
(5) Newman, C. R.; Frisbie, C. D.; da Silva Filho, D. A.; Brédas, J.-L.; Ewbank, P. C.; Mann, K. R. *Chem. Mater.* **2004**, *16*, 4436−4451.
(6) Facchetti, A. *Mater. Today* **2007**, *10*, 28−37.
(7) Subramanian, V.; Chang, P.; Lee, J.; Molesa, S.; Volkman, S. *IEEE Trans. Compon. Packag. Technol.* **2005**, *28*, 742−747.
(8) Myny, K.; Steudel, S.; Smout, S.; Vicca, P.; Furthner, F.; van der Putten, B.; Tripathi, A.; Gelinck, G.; Genoe, J.; Dehaene, W.; Heremans, P. *Org. Electron.* **2010**, *11*, 1176−1179.
(9) Riede, M.; Mueller, T.; Tress, W.; Schueppel, R.; Leo, K. *Nanotechnology* **2008**, *19*, 424001.
(10) Kippelen, B.; Brédas, J.-L. *Energy Environ. Sci.* **2009**, *2*, 251−261.
(11) Dennler, G.; Scharber, M. C.; Brabec, C. J. *Adv. Mater.* **2009**, *21*, 1323−1338.
(12) Chidichimo, G.; Filippelli, L. *Int. J. Photoenergy* **2010**, *2010*, Article ID 123534.
(13) Deibel, C.; Dyakonov, V. *Rep. Prog. Phys.* **2010**, *73*, 096401.
(14) Barth, S.; Bässler, H. *Phys. Rev. Lett.* **1997**, *79*, 4445−4448.
(15) Kirova, N.; Brazovskii, S.; Bishop, A. *Synth. Met.* **1999**, *100*, 29−53.
(16) Marks, R. N.; Halls, J. J. M.; Bradley, D. D. C.; Friend, R. H.; Holmes, A. B. *J. Phys.: Condens. Matter* **1994**, *6*, 1379.
(17) Miranda, P. B.; Moses, D.; Heeger, A. J. *Phys. Rev. B* **2001**, *64*, 081201.

(18) Kietzke, T. *Adv. OptoElectron.* **2007**, *2007*, Article ID 40285.
(19) Quarti, C.; Fazzi, D.; Tommasini, M. *Chem. Phys. Lett.* **2010**, *496*, 284−290.
(20) Galanin, M.; Khan-Magometova, S. *J. Lumin.* **1979**, *18*−*19* (Part 1), 37−40.
(21) Aaviksoo, J. *J. Lumin.* **1991**, *48*−*49* (Part 1), 57−66.
(22) Brazovskii, S.; Kirova, N. *Chem. Soc. Rev.* **2010**, *39*, 2453−2465.
(23) Tripathi, A. K.; Pflaum, J. *Appl. Phys. Lett.* **2006**, *89*, 082103.
(24) Topczak, A. K.; Roller, T.; Engels, B.; Brütting, W.; Pflaum, J. http://arxiv.org/abs/1207.1036, accessed 2012.
(25) Stehr, V.; Engels, B.; Deibel, C.; Fink, R. F. *J. Chem. Phys.* **2014**, *140*, 024503.
(26) Scholes, G. D. *Annu. Rev. Phys. Chem.* **2003**, *54*, 57−87.
(27) Brédas, J.-L.; Beljonne, D.; Coropceanu, V.; Cornil, J. *Chem. Rev.* **2004**, *104*, 4971−5003.
(28) Beljonne, D.; Hennebicq, E.; Daniel, C.; Herz, L. M.; Silva, C.; Scholes, G. D.; Hoeben, F. J. M.; Jonkheijm, P.; Schenning, A. P. H. J.; Meskers, S. C. J.; Phillips, R. T.; Friend, R. H.; Meijer, E. W. *J. Phys. Chem. B* **2005**, *109*, 10594−10604.
(29) Hennebicq, E.; Pourtois, G.; Scholes, G. D.; Herz, L. M.; Russell, D. M.; Silva, C.; Setayesh, S.; Grimsdale, A. C.; Müllen, K.; Brédas, J.-L.; Beljonne, D. *J. Am. Chem. Soc.* **2005**, *127*, 4744−4762.
(30) Poulsen, L.; Jazdzyk, M.; Communal, J.-E.; Sancho-García, J. C.; Mura, A.; Bongiovanni, G.; Beljonne, D.; Cornil, J.; Hanack, M.; Egelhaaf, H.-J.; Gierschner, J. *J. Am. Chem. Soc.* **2007**, *129*, 8585−8593.
(31) Marcus, R. A. *J. Chem. Phys.* **1956**, *129*, 966.
(32) Marcus, R. A. *Rev. Mod. Phys.* **1993**, *65*, 599−610.
(33) Barbara, P. F.; Meyer, T. J.; Ratner, M. A. *J. Phys. Chem.* **1996**, *100*, 13148−13168.
(34) Sakanoue, K.; Motoda, M.; Sugimoto, M.; Sakaki, S. *J. Phys. Chem. A* **1999**, *103*, 5551−5556.
(35) Stehr, V.; Pfister, J.; Fink, R. F.; Engels, B.; Deibel, C. *Phys. Rev. B* **2011**, *83*, 155208.
(36) Heinrich, M. A.; Pflaum, J.; Tripathi, A. K.; Frey, W.; Steigerwald, M. L.; Siegrist, T. *J. Phys. Chem. C* **2007**, *111*, 18878−18881.
(37) Dürr, A. C.; Schreiber, F.; Münch, M.; Karl, N.; Krause, B.; Kruppa, V.; Dosch, H. *Appl. Phys. Lett.* **2002**, *81*, 2276.
(38) Karl, N.; Kraft, K.-H.; Marktanner, J.; Münch, M.; Schatz, F.; Stehle, R.; Uhde, H.-M. *J. Vac. Sci. Technol. A* **1999**, *17*, 2318.
(39) Kurrle, D.; Pflaum, J. *Appl. Phys. Lett.* **2008**, *92*, 133306.
(40) May, V.; Kühn, O. *Charge and Energy Transfer Dynamics in Molecular Systems*, 3rd Edition; Wiley−VCH: Weinheim, Germany, 2011.
(41) Wong, K. F.; Bagchi, B.; Rossky, P. J. *J. Phys. Chem. A* **2004**, *108*, 5752−5763.
(42) Spano, F.; Siddiqui, S. *Chem. Phys. Lett.* **1999**, *314*, 481−487.
(43) Malagoli, M.; Coropceanu, V.; da Silva Filho, D. A.; Brédas, J. L. *J. Chem. Phys.* **2004**, *120*, 7490−7496.
(44) Duschinsky, F. *Acta Physicochim. URSS* **1937**, *7*, 551−566.
(45) Deng, W.-Q.; Goddard, W. A., III. *J. Phys. Chem. B* **2004**, *108*, 8614.
(46) Li, H.; Brédas, J.-L.; Lennartz, C. *J. Chem. Phys.* **2007**, *126*, 164704.
(47) Wen, S.-H.; Li, A.; Song, J.; Deng, W.-Q.; Han, K.-L.; Goddard, W. A., III. *J. Phys. Chem. B* **2009**, *113*, 8813−8819.
(48) Liu, Y.-H.; Xie, Y.; Lu, Z.-Y. *Chem. Phys.* **2010**, *367*, 160−166.
(49) Sancho-García, J. C.; Pérez-Jiménez, A. J. *J. Chem. Phys.* **2008**, *129*, 024103.
(50) Sancho-García, J. C.; Pérez-Jiménez, A. J.; Olivier, Y.; Cornil, J. *Phys. Chem. Chem. Phys.* **2010**, *12*, 9381−9388.
(51) Sancho-García, J. C.; Pérez-Jiménez, A. J. *Phys. Chem. Chem. Phys.* **2009**, *11*, 2741−2746.
(52) Beljonne, D.; Curutchet, C.; Scholes, G. D.; Silbey, R. J. *J. Phys. Chem. B* **2009**, *113*, 6583−6599.
(53) Kimura, A.; Kakitani, T.; Yamato, T. *J. Phys. Chem. B* **2000**, *104*, 9276−9287.
(54) Fückel, B.; Köhn, A.; Harding, M. E.; Diezemann, G.; Hinze, G.; Basché, T.; Gauss, J. *J. Chem. Phys.* **2008**, *128*, 074505.
(55) Norton, J. E.; Brédas, J.-L. *J. Am. Chem. Soc.* **2008**, *130*, 12377−12384.
(56) McMahon, D. P.; Troisi, A. *J. Phys. Chem. Lett.* **2010**, *1*, 941−946.
(57) Einstein, A. *Ann. Phys.* **1905**, *322*, 549−560.
(58) von Smoluchowski, M. *Ann. Phys.* **1906**, *326*, 756−780.
(59) Houili, H.; Tutiš, E.; Batistić, I.; Zuppiroli, L. *J. Appl. Phys.* **2006**, *100*, 033702.
(60) Di Donato, E.; Fornari, R. P.; Di Motta, S.; Li, Y.; Wang, Z.; Negri, F. *J. Phys. Chem. B* **2010**, *114*, 5327−5334.
(61) Rosso, K.; Dupuis, M. *Theor. Chem. Acc.* **2006**, *116*, 124−136.
(62) Sánchez-Carrera, R. S.; Coropceanu, V.; da Silva Filho, D. A.; Friedlein, R.; Osikowicz, W.; Murdey, R.; Suess, C.; Salaneck, W. R.; Brédas, J.-L. *J. Phys. Chem. B* **2006**, *110*, 18904−18911.
(63) Grimme, S. *J. Chem. Phys.* **2003**, *118*, 9095.
(64) Hellweg, A.; Grün, S. A.; Hättig, C. *Phys. Chem. Chem. Phys.* **2008**, *10*, 4119−4127.
(65) Christiansen, O.; Koch, H.; Jørgensen, P. *Chem. Phys. Lett.* **1995**, *243*, 409−418.
(66) Hättig, C.; Weigend, F. *J. Chem. Phys.* **2000**, *113*, 5154.
(67) Hättig, C. *J. Chem. Phys.* **2003**, *118*, 7751.
(68) Köhn, A.; Hättig, C. *J. Chem. Phys.* **2003**, *119*, 5021.
(69) Dirac, P. A. M. *Proc. R. Soc. London A* **1929**, *123*, 714−733.
(70) Slater, J. C. *Phys. Rev.* **1951**, *81*, 385−390.
(71) Vosko, S. H.; Wilk, L.; Nusair, M. *Can. J. Phys.* **1980**, *58*, 1200−1211.
(72) Becke, A. D. *Phys. Rev. A* **1988**, *38*, 3098−3100.
(73) Lee, C.; Yang, W.; Parr, R. G. *Phys. Rev. B* **1988**, *37*, 785−789.
(74) Becke, A. D. *J. Chem. Phys.* **1993**, *98*, 5648.
(75) Eichkorn, K.; Treutler, O.; Öhm, H.; Häser, M.; Ahlrichs, R. *Chem. Phys. Lett.* **1995**, *240*, 283−290.
(76) Eichkorn, K.; Weigend, F.; Treutler, O.; Ahlrichs, R. *Theor. Chem. Acc.* **1997**, *97*, 119−124.
(77) Weigend, F. *Phys. Chem. Chem. Phys.* **2006**, *8*, 1057−1065.
(78) Dunning, T. H. *J. Chem. Phys.* **1989**, *90*, 1007.
(79) Ahlrichs, R.; Bär, M.; Häser, M.; Horn, H.; Kölmel, C. *Chem. Phys. Lett.* **1989**, *162*, 165−169.
(80) TURBOMOLE GmbH. *TURBOMOLE V6.2, a development of University of Karlsruhe and Forschungszentrum Karlsruhe GmbH, 1989−2007*. Available via the Internet at http://www.turbomole.com, accessed 2010.
(81) Kasha, M. *Discuss. Faraday Soc.* **1950**, *9*, 14−19.
(82) Fink, R.; Pfister, J.; Schneider, A.; Zhao, H.; Engels, B. *Chem. Phys.* **2008**, *343*, 353−361.
(83) Fink, R. F.; Pfister, J.; Zhao, H. M.; Engels, B. *Chem. Phys.* **2008**, *346*, 275−285.
(84) Davydov, A. S. *Sov. Phys.—Usp.* **1964**, *7*, 145.
(85) Hättig, C.; Köhn, A. *J. Chem. Phys.* **2002**, *117*, 6939.
(86) Schirmer, J. *Phys. Rev. A* **1982**, *26*, 2395−2416.
(87) Christiansen, O.; Jørgensen, P.; Hättig, C. *Int. J. Quantum Chem.* **1998**, *68*, 1−52.
(88) Christiansen, O.; Bak, K. L.; Koch, H.; Sauer, S. P. *Chem. Phys. Lett.* **1998**, *284*, 47−55.
(89) Trofimov, A. B.; Stelter, G.; Schirmer, J. *J. Chem. Phys.* **2002**, *117*, 6402.
(90) Liu, W.; Settels, V.; Harbach, P. H. P.; Dreuw, A.; Fink, R. F.; Engels, B. *J. Comput. Chem.* **2011**, *32*, 1971−1981.
(91) González, L.; Escudero, D.; Serrano-Andrés, L. *ChemPhysChem* **2012**, *13*, 28−51.
(92) Schon, C.; Roth, W.; Fischer, I.; Pfister, J.; Kaiser, C.; Fink, R. F.; Engels, B. *Phys. Chem. Chem. Phys.* **2010**, *12*, 9339−9346.
(93) Settels, V.; Liu, W.; Pflaum, J.; Fink, R. F.; Engels, B. *J. Comput. Chem.* **2012**, *33*, 1544−1553.
(94) Schon, C.; Roth, W.; Fischer, I.; Pfister, J.; Fink, R. F.; Engels, B. *Phys. Chem. Chem. Phys.* **2011**, *13*, 11076−11082.
(95) Pfister, J.; Schon, C.; Roth, W.; Kaiser, C.; Lambert, C.; Gruss, K.; Braunschweig, H.; Fischer, I.; Fink, R. F.; Engels, B. *J. Phys. Chem. A* **2011**, *115*, 3583−3591.
(96) Stewart, R. F. *J. Phys. B* **1975**, *8*, 1.

(97) Hellweg, A. *J. Chem. Phys.* **2011**, *134*, 064103.
(98) Grimme, S.; Parac, M. *ChemPhysChem* **2003**, *4*, 292−295.
(99) Cai, Z.-L.; Sendt, K.; Reimers, J. R. *J. Chem. Phys.* **2002**, *117*, 5543.
(100) Paddon-Row, M. N.; Shephard, M. J. *J. Phys. Chem. A* **2002**, *106*, 2935−2944.
(101) Dreuw, A.; Head-Gordon, M. *J. Am. Chem. Soc.* **2004**, *126*, 4007−4016.
(102) Dreuw, A.; Head-Gordon, M. *Chem. Rev.* **2005**, *105*, 4009−4037.
(103) Padgett, C. W.; Arman, H. D.; Pennington, W. T. *Cryst. Growth Des.* **2007**, *7*, 367−372.
(104) Brock, C. P.; Dunitz, J. D. *Acta Crystallogr., Sect. B: Struct. Sci.* **1990**, *46*, 795−806.
(105) George, G.; Morris, G. *J. Mol. Spectrosc.* **1968**, *26*, 67−71.
(106) Huebner, R.; Meilczarek, S.; Kuyatt, C. *Chem. Phys. Lett.* **1972**, *16*, 464−469.
(107) McConkey, J. W.; Trajmar, S.; Man, K. F.; Ratliff, J. M. *J. Phys. B* **1992**, *25*, 2197.
(108) Furche, F.; Ahlrichs, R. *J. Chem. Phys.* **2002**, *117*, 7433−7447.
(109) Hout, R. F.; Levi, B. A.; Hehre, W. J. *J. Comput. Chem.* **1982**, *3*, 234−250.
(110) Scott, A. P.; Radom, L. *J. Phys. Chem.* **1996**, *100*, 16502−16513.
(111) Klevens, H. B.; Platt, J. R. *J. Chem. Phys.* **1949**, *17*, 470.
(112) Kutzelnigg, W. *Einführung in die Theoretische Chemie*, 2nd Edition; Wiley−VCH: Weinheim, Germany, 1993.
(113) Speight, J.; Lange, N. A. *Lange's Handbook of Chemistry*, 16th Edition; McGraw−Hill: New York, 2005.
(114) Galanin, M. D.; Chizhikova, Z. A. *Opt. Spectrosc.* **1961**, *11*, 143.
(115) Birks, J. B.; King, T. A.; Munro, I. H. *Proc. Phys. Soc.* **1962**, *80*, 355.
(116) Powell, R. C.; Soos, Z. G. *J. Lumin.* **1975**, *11*, 1−45.
(117) Heisel, F.; Miehe, J. A.; Schott, M.; Sipp, B. *Mol. Cryst. Liq. Cryst.* **1978**, *41*, 251−255.
(118) Lambert, W. R.; Felker, P. M.; Syage, J. A.; Zewail, A. H. *J. Chem. Phys.* **1984**, *81*, 2195.
(119) Steiner, R. P.; Michl, J. *J. Am. Chem. Soc.* **1978**, *100*, 6861−6867.
(120) Bergman, A.; Jortner, J. *Chem. Phys. Lett.* **1972**, *15*, 309−315.
(121) Meth, J. S.; Marshall, C.; Fayer, M. *Solid State Commun.* **1990**, *74*, 281−284.
(122) Mulder, B. J. *Philips Res. Rep.* **1967**, *22*, 142.
(123) Donati, D.; Williams, J. O. *Mol. Cryst. Liq. Cryst.* **1978**, *44*, 23−32.
(124) Birks, J. B. *Proc. Phys. Soc.* **1962**, *79*, 494.
(125) Birks, J. B. *Mol. Cryst. Liq. Cryst.* **1974**, *28*, 117−129.
(126) Kepler, R. G.; Merrifield, R. E. *J. Chem. Phys.* **1964**, *40*, 1173.
(127) Cohen, M. D.; Klein, E.; Ludmer, Z. *Chem. Phys. Lett.* **1976**, *37*, 611−613.
(128) Heinemeyer, U.; Scholz, R.; Gisslén, L.; Alonso, M. I.; Ossó, J. O.; Garriga, M.; Hinderhofer, A.; Kytka, M.; Kowarik, S.; Gerlach, A.; Schreiber, F. *Phys. Rev. B* **2008**, *78*, 085210.
(129) Lunkenheimer, B.; Köhn, A. Simulation of exciton transport in amorphous organic semiconductors, Poster 131. Presented at the *49th Symposium on Theoretical Chemistry (STC Erlangen)*, Erlangen, Germany, October 2013.